Near real-time simulations of global CMT earthquakes

Jeroen Tromp,[1] Dimitri Komatitsch,[2,3] Vala Hjörleifsdóttir,[4]* Qinya Liu,[5] Hejun Zhu,[6] Daniel Peter,[6] Ebru Bozdag,[6] Dennis McRitchie,[7] Paul Friberg,[8] Chad Trabant[9] and Alex Hutko[9]

[1]*Department of Geosciences and Program in Applied & Computational Mathematics, Princeton University, Princeton, NJ, USA.*
E-mail: jtromp@princeton.edu
[2]*Université de Pau et des Pays de l'Adour, CNRS & INRIA Magique-3D, Laboratoire de Modélisation et d'Imagerie en Géosciences UMR 5212, Pau, France*
[3]*Institut universitaire de France, 103 boulevard Saint-Michel, 75005 Paris, France*
[4]*Lamont-Doherty Earth Observatory, Columbia University, New York, NY, USA*
[5]*Department of Physics, University of Toronto, Ontario, Canada*
[6]*Department of Geosciences, Princeton University, Princeton, NJ, USA*
[7]*Princeton Institute for Computational Science & Engineering, Princeton University, Princeton, NJ, USA*
[8]*Instrumental Software Technologies, Inc., New Paltz, NY, USA*
[9]*IRIS DMC, Seattle, Washington, USA*

GJI Seismology

SUMMARY

We have developed a near real-time system for the simulation of global earthquakes. Prompted by a trigger from the Global Centroid Moment Tensor (CMT) Project, the system automatically calculates normal-mode synthetic seismograms for the Preliminary Reference Earth Model, and spectral-element synthetic seismograms for 3-D mantle model S362ANI in combination with crustal model Crust2.0. The 1-D and 3-D synthetics for more than 1800 seismographic stations operated by members of the international Federation of Digital Seismograph Networks are made available via the internet (global.shakemovie.princeton.edu) and the Incorporated Research Institutions for Seismology Data Management Center (IRIS; iris.edu). The record length of the synthetics is 100 min for CMT events with magnitudes less than 7.5, capturing R1 and G1 at all epicentral distances, and 200 min for CMT events with magnitudes equal to or greater than 7.5, capturing R2 and G2. The mode simulations are accurate at periods of 8 s and longer, whereas the spectral-element simulations are accurate between periods from 17 to 500 s. The spectral-element software incorporates a number of recent improvements, for example, the mesh honours the Moho as a first-order discontinuity underneath the oceans and continents, and the performance of the solver is enhanced by reducing processor cache misses and optimizing matrix–matrix multiplication. In addition to synthetic seismograms, the system produces a number of earthquake animations, as well as various record sections comparing simulated and observed seismograms.

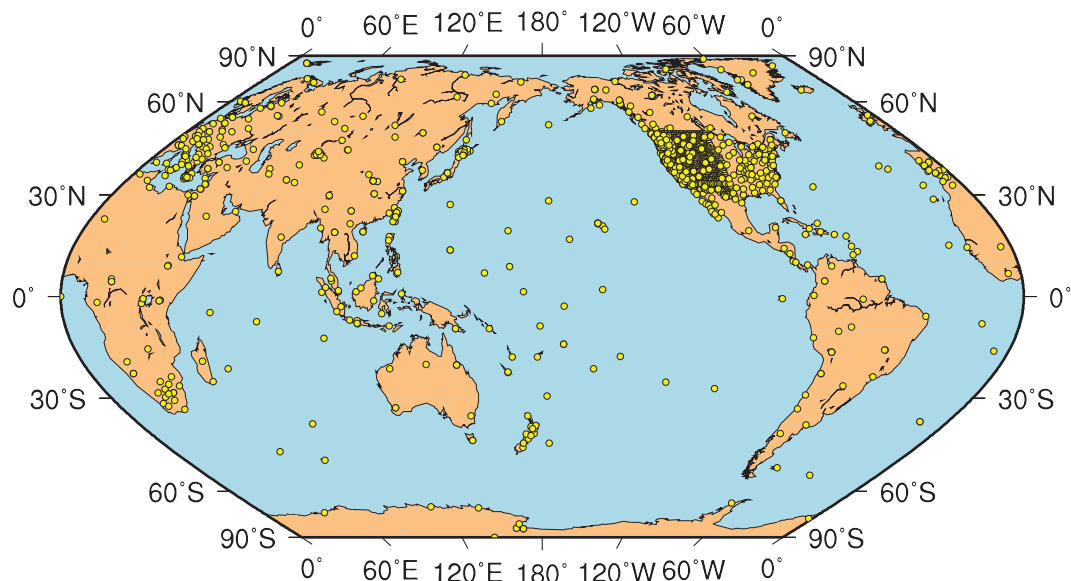**Key words:** Earthquake ground motions; Seismicity and tectonics; Computational seismology.

1 INTRODUCTION

The members of the international Federation of Digital Seismograph Networks (FDSN) collectively provide access to three-component, broad-band time-series of ground motion recorded at hundreds of locations around the world. Freely available data from these cooperative networks are used, among other things, to detect, monitor, and characterize earthquake activity, and to image Earth's interior.

For stations which are online, data are accessible in real time. The purpose of the near real-time system presented in this paper is to provide seismologists with synthetic seismograms that complement the data recorded by the FDSN.

Every week, of order ten magnitude ∼5.5 and greater earthquakes occur somewhere in the world. Using data recorded by the FDSN, the source characteristics of such earthquakes, for example, origin time, hypocentre, magnitude and fault-plane orientation, are routinely determined by a number of organizations. For example, the National Earthquake Information Center (NEIC) of the United States Geological Survey (USGS) determines global earthquake hypocentres and magnitudes. The Global CMT Project (globalCMT.org) uses NEIC earthquake information to determine a

*Now at: Instituto de Geofísica, Universidad Nacional Autónoma de Mexico, Circuito de la Investigación Científica s/n, Ciudad Universitaria, D.F. 04510 Distrito Federal, México.

Figure 1. Map showing locations of 1838 seismographic stations supported by members of the FDSN (yellow dots). At each of these locations, the near real-time system provides three-component normal-mode synthetics for the 1-D PREM (Dziewoński & Anderson 1981) and SEM synthetics for 3-D model S362ANI (Kustowski *et al.* 2008) plus Crust2.0 (Bassin *et al.* 2000). The synthetics capture R1 and G1 at all epicentral distances for CMT events with $M_w < 7.5$, and R2 and G2 for CMT events with $M_w \geq 7.5$.

Centroid Moment Tensor (CMT) solution (Dziewoński *et al.* 1981; Dziewoński & Woodhouse 1983), which contains information about timing, hypocentre, magnitude, duration and fault-plane orientation of an event. The NEIC information is typically available within minutes, and the CMT solution within a day. The CMT catalogue contains tens of thousands of earthquakes with magnitudes greater than ~5.5, and is widely used by geophysicists throughout the world.

Seismologists also use data recorded by the FDSN to image Earth's structure. Initially, this involved determining spherically symmetric, 1-D models of Earth. For example, the widely used Preliminary Reference Earth Model (PREM) was determined by Dziewoński & Anderson in 1981. Over the past 30 yr, seismologists have refined tomographic techniques to map 3-D variations in Earth's interior (e.g. Dziewoński *et al.* 1977; Woodhouse & Dziewoński 1984; Grand *et al.* 1997; Montelli *et al.* 2004). Such maps reflect thermal and compositional heterogeneity in Earth's mantle and inner core. At long wavelengths, tomographic images determined by different research groups are in reasonably good agreement (e.g. Dziewoński & Romanowicz 2007).

Inversions for source parameters or Earth structure generally involve a comparison between observed and simulated seismograms, for example, waveform differences or cross-correlation traveltime anomalies. The purpose of the near real-time system discussed in this paper is to provide the necessary 1-D and/or 3-D reference synthetics. For purposes of education and outreach, the system also produces an animation of each earthquake in the form of a movie of the velocity wavefield on Earth's surface.

2 SYNTHETIC SEISMOGRAMS

The near real-time system computes two sets of synthetic seismograms, which we briefly describe in the following two sections. The record length is 100 min for earthquakes with magnitudes less than 7.5, such that the first arriving Love and Rayleigh waves are included in the seismograms at all epicentral distances. For earth-

quakes with magnitudes of 7.5 and greater, the record length is 200 min, thereby incorporating one complete surface wave orbit at all epicentral distances. We currently calculate synthetic seismograms at 1838 stations supported by members of the FDSN (Fig. 1).
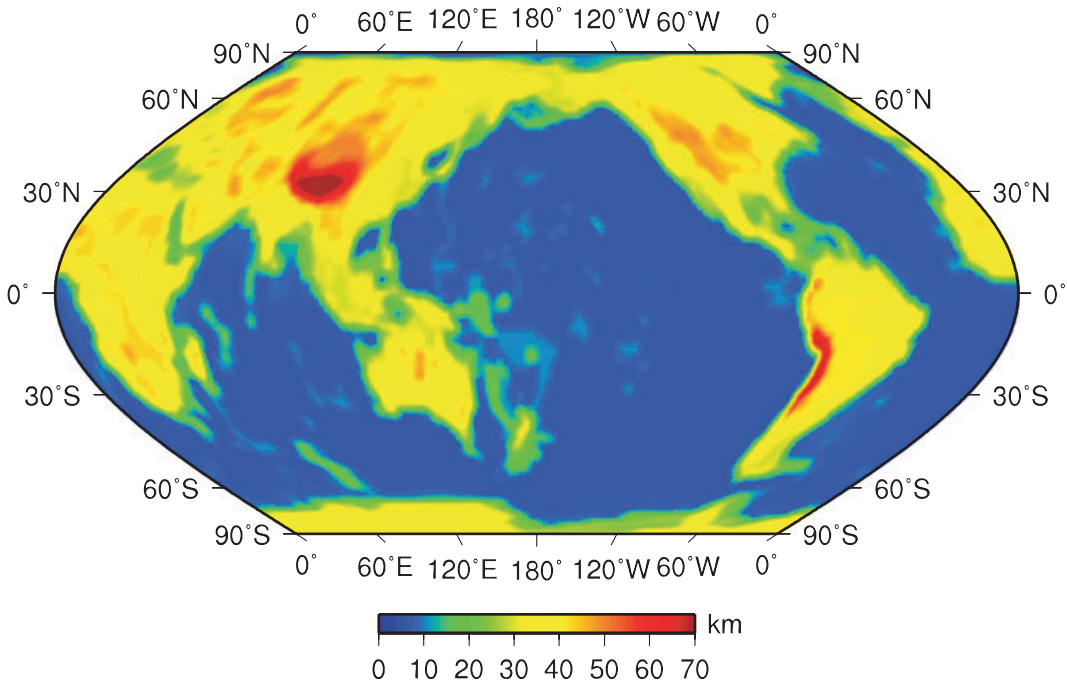
2.1 Normal-mode seismograms

Semi-analytical techniques for the calculation of synthetic seismograms for spherically symmetric earth models are widely available. For example, broadband synthetic seismograms, containing information about short-period body waves as well as long-period surface waves, may be calculated based upon normal-mode summation (see e.g. Gilbert 1971; Dahlen & Tromp 1998). This approach involves summing the free oscillations of a spherically symmetric earth model up to a certain period. For spherically symmetric earth model PREM (Dziewoński & Anderson 1981), we calculate synthetic seismograms based upon normal-mode summation. These mode synthetic are accurate at periods of 8 s and longer.

2.2 Spectral-element seismograms

The simulation of broadband global seismic wave propagation in 3-D earth models has only recently become practical. The numerical technique we have developed and implemented is based upon a spectral-element method (SEM), which combines the flexibility of the finite-element method with the accuracy of the global pseudospectral method (Komatitsch & Vilotte 1998; Komatitsch & Tromp 1999, 2002a,b; Chaljub *et al.* 2003). Its main advantage for parallel computing purposes is an exactly diagonal mass matrix. Although the calculation of synthetic seismograms for 1-D earth models is relatively straightforward and numerically fast and cheap, the calculation of 3-D synthetics requires access to modest to large parallel computers.

The near real-time system computes spectral-element synthetic seismograms for 3-D mantle model S362ANI (Kustowski *et al.* 2008) in combination with crustal model Crust2.0 (Bassin *et al.*

Figure 2. Map of crustal thickness obtained by smoothing $2° \times 2°$ block model Crust2.0 (Bassin *et al.* 2000) with a one-degree Gaussian cap. The Moho is honored in the spectral-element mesh as a first-order discontinuity if the crustal thickness is less than 15 km (one spectral element) or greater than 35 km (two spectral elements), as shown in Fig. 3.

2000). This is the same 3-D model as is currently used by the Global CMT Project. The simulations incorporate effects due to attenuation based upon 1-D model QL6 (Durek & Ekström 1996), rotation, and self-gravitation in the Cowling approximation[1] (Dahlen & Tromp 1998; Komatitsch & Tromp 2002a,b). We use domain decomposition between the liquid outer core and the solid inner core and mantle. The spectral-element mesh honours all first- and second-order mantle discontinuities in 1-D reference model STW105 (Kustowski *et al.* 2008). Earth's ellipticity is accommodated by turning all first- and second-order discontinuities in the 1-D reference model into ellipsoids based upon Clairaut's equation, and adjusting the 1-D model parameters (density, wave speeds and attenuation) accordingly (see e.g. Dahlen & Tromp 1998, section 14.1). Topography and bathymetry of Earth's surface are accommodated by stretching the mesh near the surface based upon an approach developed by Lee *et al.* (2008).

2.2.1 Implementation of the crust

Lateral variations in crustal thickness are provided by model Crust2.0 (Bassin *et al.* 2000), a $2° \times 2°$ block model. We smooth this model with a $1°$ Gaussian cap; the resulting map of crustal thickness is shown in Fig. 2. The crust of the 1-D reference model is removed and replaced by mantle, which is subsequently overprinted by Crust2.0. We incorporate sedimentary layers in Crust.2.0 if sediment thickness is 2 km or greater. We have developed a new mesh implementation that honors the Moho if the crustal thickness is less than 15 km (one spectral element) or greater than 35 km (two spectral elements), as illustrated in Fig. 3. In transition regions, shown by the white areas in Fig. 3, the Moho is not honoured by the
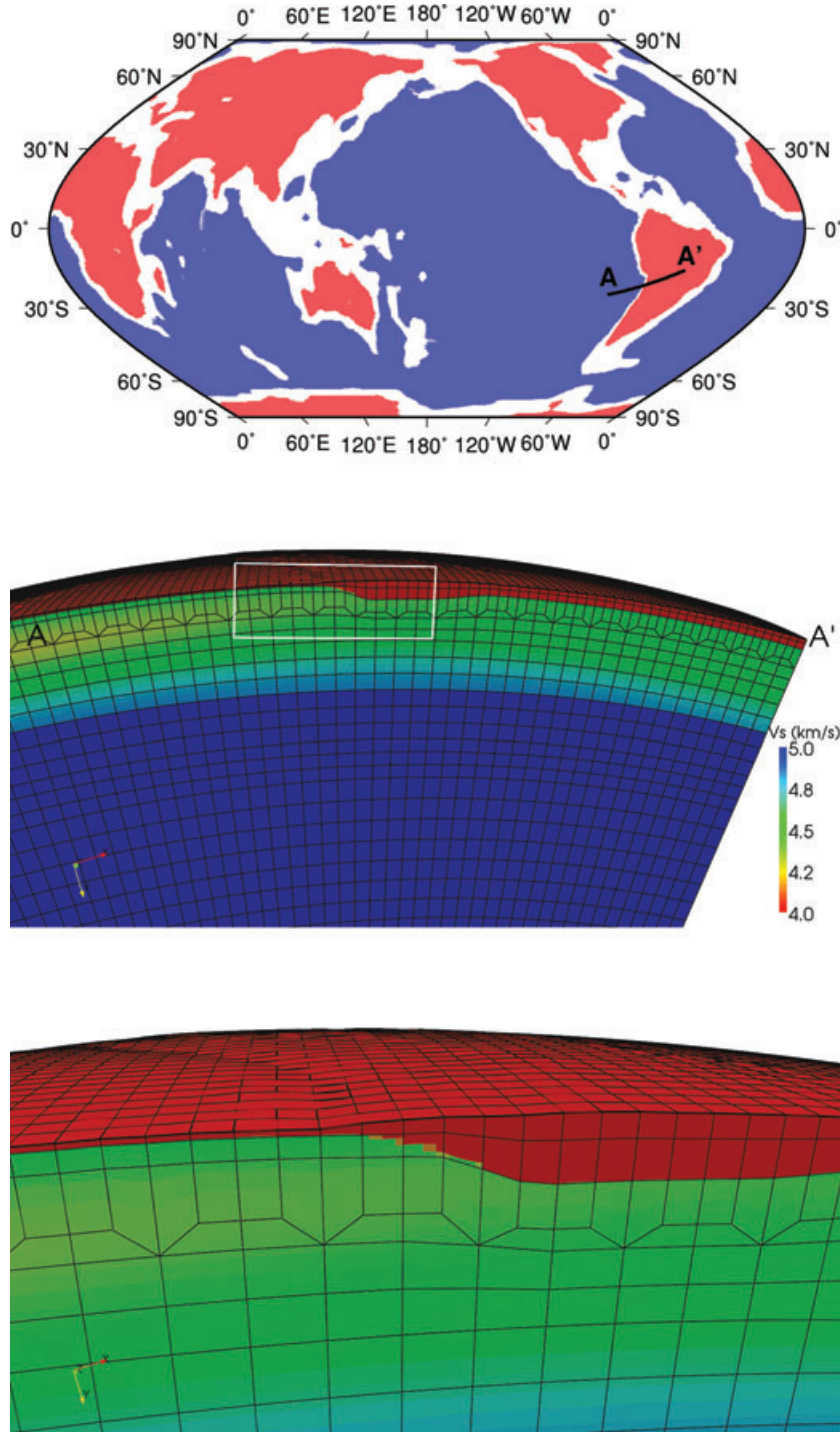
mesh. In that case the discontinuity runs across the spectral elements and is captured by the Gauss–Lobatto–Legendre (GLL) integrations points (125 GLL points per element). When a discontinuity is not honored by the mesh, the SEM behaves like any other method based upon a strong formulation of the seismic wave equation, for example, finite-difference or pseudospectral methods, capturing model transitions as staircases at the GLL level.

In Fig. 4, we compare 3-D SEM synthetics for various spectral-element meshes and the implementation of the crust illustrated in Fig. 3 along predominantly continental or oceanic paths, respectively. If the mesh honours the Moho, there should be no notable differences between SEM synthetics based upon different meshes, as long as the records are filtered within a common range of validity. Because we do not honour the Moho everywhere, as illustrated in Fig. 3, there are very minor visible differences between simulations based upon 160 spectral elements along a 90° surface arc, and simulations based upon 256 or 320 spectral elements, which are virtually indistinguishable. Note that, for a model with discontinuities, 3-D simulations based upon a strong method always show slight differences between synthetics corresponding to different grid resolutions, filtered within a common range of validity, simply because each grid samples the discontinuities slightly differently.

2.2.2 Implementation of topography & bathymetry

We incorporate surface topography and bathymetry in the mesh based upon model ETOPO1 (Amante & Eakins 2009), which has a resolution of 1 arcmin. The top face of a finite-element at Earth's surface contains $3 \times 3 = 9$ anchors, each of which is used to capture topography. For a 3-D simulation accurate at periods between 17 s and ~500 s, the number of spectral elements along a great circle equals $\sim 4 \times 256 = 1024$, giving a nominal resolution of ~27 km (using the largest distance between a given surface anchor and its

---

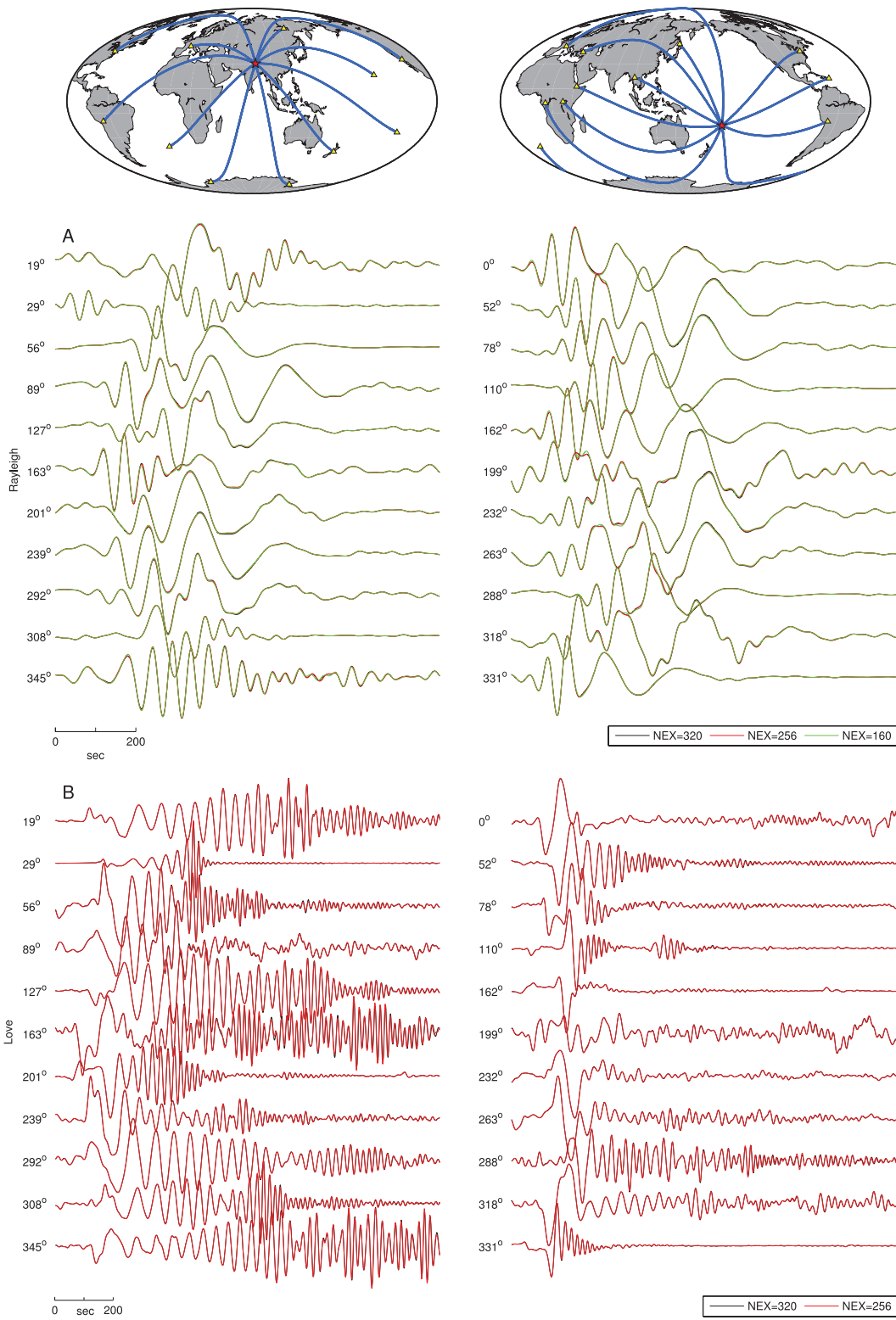[1] This imposes the 500 s long-period upper bound.

Figure 3. Top: The Moho is honored in the spectral-element mesh as a first-order discontinuity if the crustal thickness is less than 15 km (blue areas) or greater than 35 km (red areas). In the white transition regions, the Moho runs across the spectral elements; in this case model variations are captured by the Gauss–Lobatto–Legendre (GLL) integration points ($5 \times 5 \times 5 = 125$ GLL points per element). Middle: cross section along profile AA' (indicated in the top map) showing the spectral-element mesh and lateral variations in shear wave speed. When the crust is more than 35 km thick, the Moho is honoured as a first-order discontinuity in the mesh by two layers of spectral elements, and when the crust is less than 15 km thick, the crust is captured by a thin, single layer of elements. Bottom: zoom in on the region indicated by the white box in the middle figure.

nearest surface neighbours).[2] Fig. 5 illustrates how topography and bathymetry in South America are captured by the mesh.
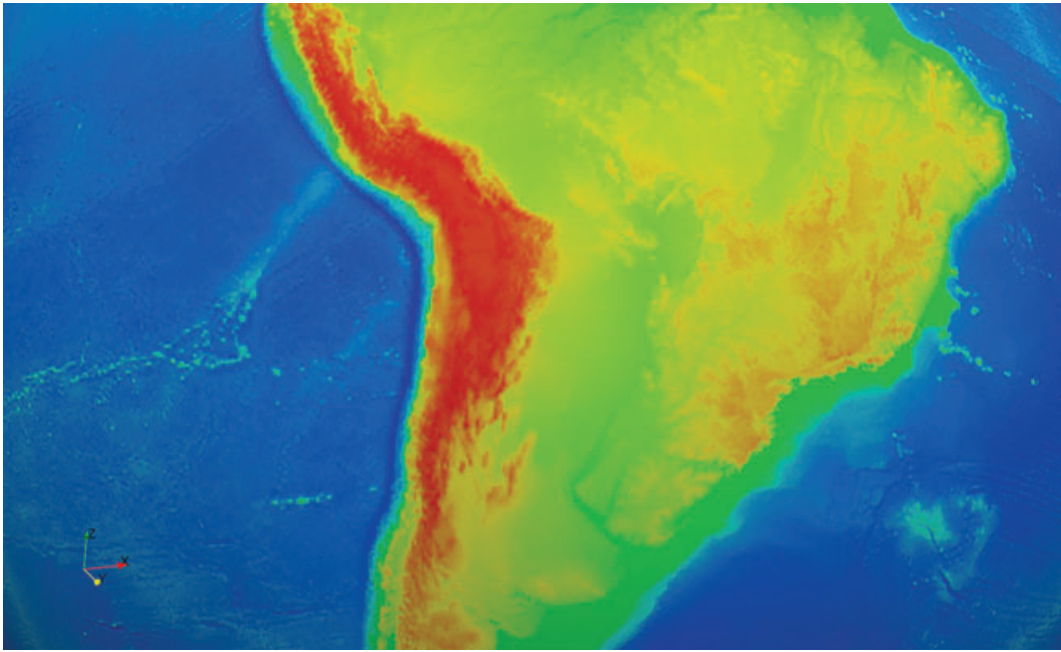
---

[2] Note that the average GLL grid spacing is ∼14 km at Earth's surface.

2.2.3 Improvements in performance

In order to increase performance and reduce simulation times, the software has been further optimized in two main ways: reducing processor cache misses and optimizing matrix–matrix multiplications.
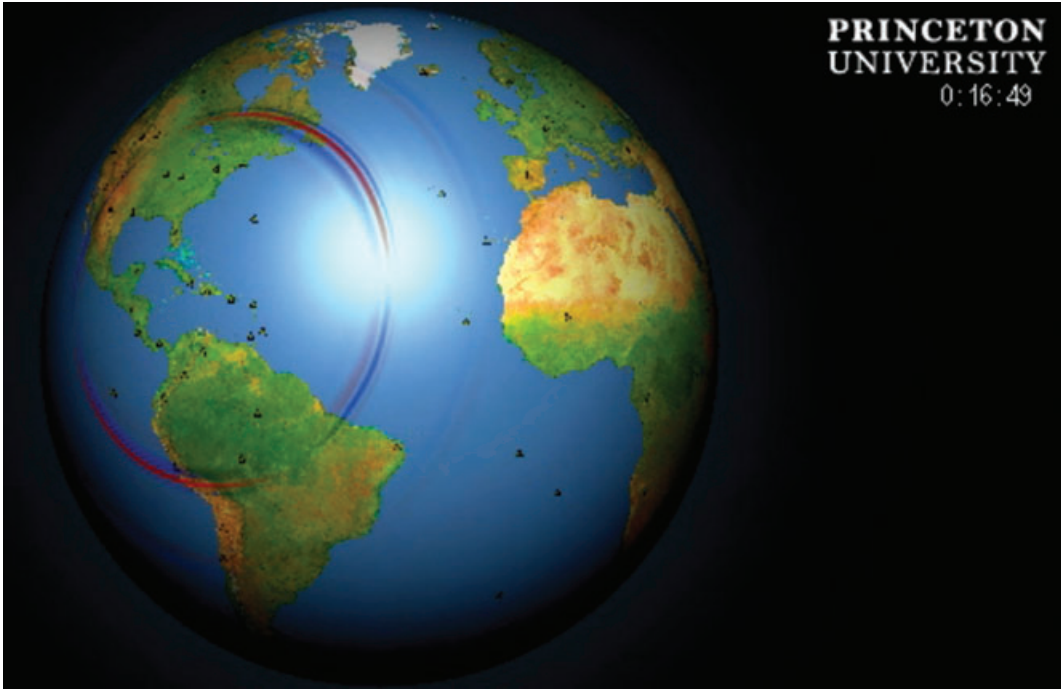
Figure 4. Comparison of 3-D SEM synthetics for various spectral-element meshes and the implementation of the crust illustrated in Fig. 3. Black/red/green synthetics involve 320/256/160 spectral elements along a 90° surface arc, respectively. Source azimuth is plotted to the left of each set of traces. Top left map: predominantly continental surface wave ray paths for the 2005 April 7, $M_w = 6.3$, Xizang earthquake (depth of 12 km). Top right map: predominantly oceanic surface wave ray paths for the 2010 February 4, $M_w = 5.6$, Tonga earthquake (depth of 25 km). (a) Vertical component 3-D SEM synthetics aligned on Rayleigh waves (using a 3.8 km s^{-1} phase speed), plotted as a function of source azimuth, and bandpass filtered between 40 and 400 s. Left- and right-hand columns correspond to the predominantly continental and oceanic paths shown in the top maps. (b) Transverse component 3-D SEM synthetics aligned on Love waves (using a 4.4 km s^{-1} phase speed), plotted as a function of source azimuth, and bandpass filtered between 17 and 400 s. Left- and right-hand columns correspond to the predominantly continental and oceanic paths shown in the top maps. Slight differences between sets of synthetics are due to the white crustal transition regions not honored by the spectral-element mesh, as shown in Fig. 3.
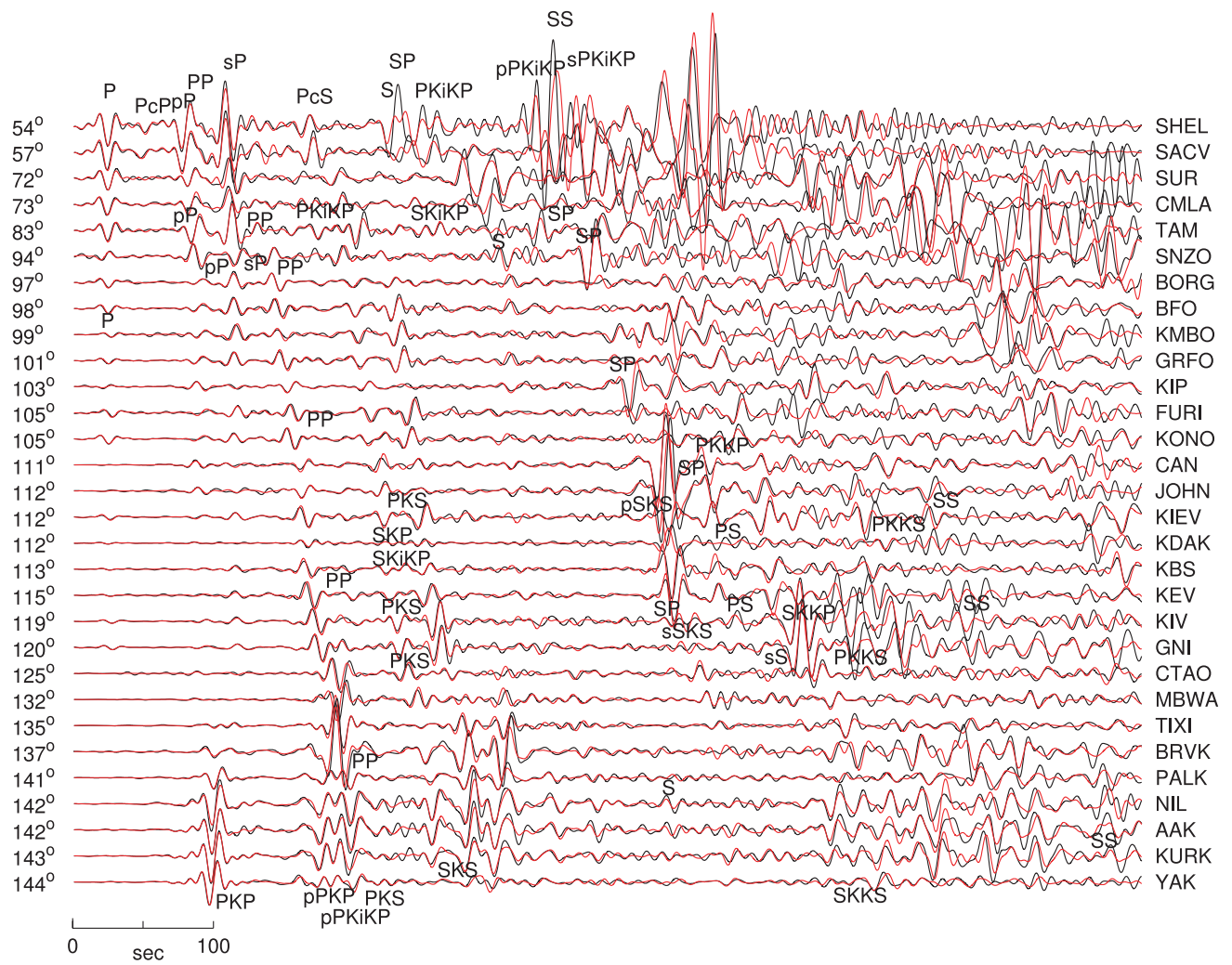
Figure 5. Each spectral element at the Earth's surface has $3 \times 3 = 9$ finite-element anchors in its top face, and these are used to capture topography and bathymetry. Shown are surface elevations in South America as captured by the spectral-element mesh used in the near real-time 3-D SEM simulations.

The first optimization minimizes processor cache misses, which can strongly decrease performance. Current CPU architectures make use of different cache levels to increase the number of floating-point operations per second. Especially beneficial is the data cache, which has very short data array access times (i.e. low latency). Cache misses occur every time instructions attempt to access array variables that are not currently stored in the data cache. Reloading the cache costs time, thereby reducing the per-

formance of the software. New software routines improve data cache usage by reducing the number of cache misses (Komatitsch *et al.* 2008). The approach optimizes the ordering scheme of the global indirect addressing array that maps local grid points to unique global degrees of freedom (Komatitsch & Tromp 2002a)—which is heavily accessed in spectral-element implementations—in such a way that accessing global array variables becomes more efficient.

Figure 6. Snapshot of a spectral-element simulation of the 2010 January 12, $M_w = 7.1$ Haiti earthquake. The near real-time system produces animations of all earthquakes reported by the Global CMT Project. The animations show the velocity wavefield on Earth's surface as a function of time. Red: upward motion; Blue: downward motion. The prominent waves are the Rayleigh surface waves, and one can vaguely see *SS* waves crossing, e.g. Greenland.

Figure 7. Vertical component record section comparing data (black) and SEM synthetics (red) for the 2008 September 3, $M_w = 6.3$ Santiago del Estero, Argentina earthquake, which occurred at a depth of 571 km. The records are aligned on the *P* wave, plotted as a function of epicentral distance, and bandpass filtered between 17 and 60 s. Major seismological body wave arrivals are labelled. Epicentral distance is plotted to the left of each set of traces, and FDSN station identification codes are plotted to the right.

Further performance improvements are obtained by using optimized matrix–matrix multiplication schemes inside each spectral element, since the most time consuming part of the SEM algorithm involves multiplying small matrices that contain the local value of a given field with local derivative matrices. These matrices have a size of 5 × 5 GLL points and are therefore too small to efficiently resort to optimized matrix multiplication libraries, such as BLAS3, but Deville *et al.* (2002) developed an optimal implementation in which small loops are unrolled, restructured and inlined in order to minimize the number of memory accesses and significantly increase the number of floating-point operations performed per memory access. We note that graphics processing units (GPUs) may be used in the near future to further increase performance in a spectral-element code (Komatitsch *et al.* 2009, 2010).

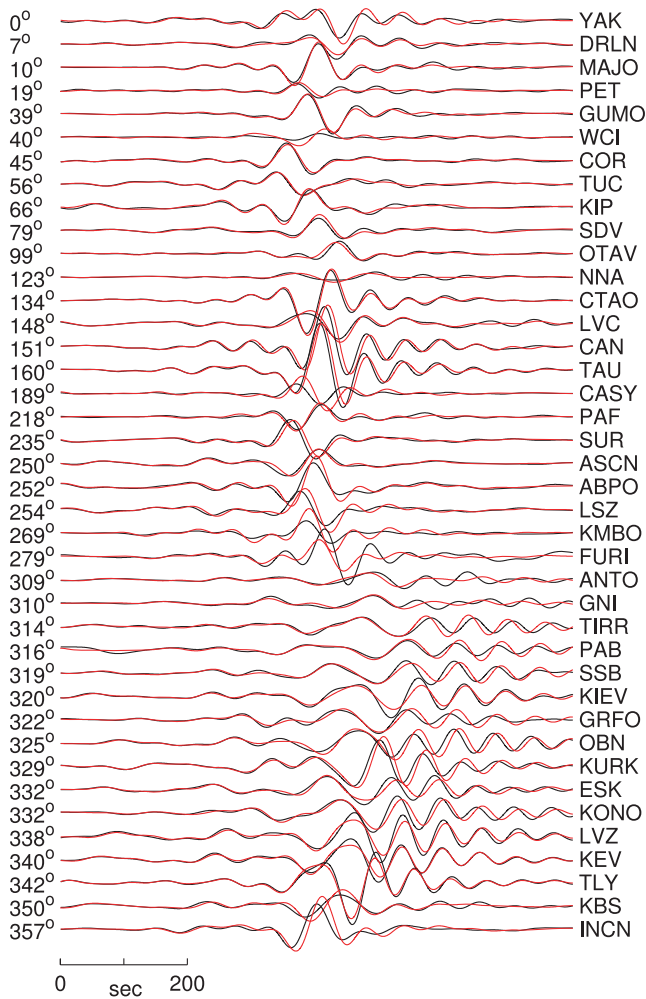## 3 ANIMATIONS AND RECORD SECTIONS

After each event, the near real-time system performs a low-resolution 3-D spectral-element simulation to produce an animation of the earthquake. The duration of the simulation scales linearly with the size of the earthquake. The movies show the velocity wavefield on Earth's surface as a function of time, as illustrated by the snapshot shown in Fig. 6 for the 2010 January 12, Haiti earthquake.

Fig. 7 shows a record section comparison between data and SEM synthetics for the deep (depth of 571 km) 2003 September 3, $M_w = 6.3$, Santiago del Estero, Argentina earthquake. The vertical component seismograms are aligned on the *P* wave, plotted as a function of epicentral distance, and bandpass filtered between 17 and 60 s. Fig. 8 shows a transverse component record section of observed and simulated Love waves as a function of source azimuth for the shallow (depth of 21 km) 2007 August 17, $M_w = 6.4$, Banda Sea earthquake. The records are bandpass filtered between 60 and 200 s. The remaining differences between SEM simulations and corresponding data may be used to improve earthquake source parameters and 3-D seismological models of Earth's interior.

4 DISCUSSION

Each time an earthquake of magnitude ~5.5 or greater occurs anywhere in the world, we use a trigger from the Global CMT Project to initiate calculations of 1-D and 3-D synthetic seismograms. For

Figure 8. Transverse component record section comparing data (black) and SEM synthetics (red) for the 2007 August 17, $M_\mathrm{w} = 6.4$, Banda Sea earthquake, which occurred at a depth of 21 km. The records are aligned on the Love wave (using a 4.4 km s^{-1} phase speed), plotted as a function of source azimuth, and bandpass filtered between 60 and 200 s. Source azimuth is plotted to the left of each set of traces, and FDSN station identification codes are plotted to the right.

the 1-D simulation we use mode summation for 1-D PREM, and for the 3-D simulation we use the SEM for 3-D model S362ANI plus Crust2.0. The 1-D and 3-D synthetic seismograms and various animations are made available in near real-time via the web server global.shakemovie.princeton.edu, and soon also through the IRIS Data Management System (iris.edu/data).

Time permitting, the system will be used to analyse past earthquakes. The CMT catalogue contains tens of thousands of entries, and any available spare compute cycles will be used for the analysis of past events, such that, ultimately, 1-D and 3-D synthetics for all earthquakes in the CMT catalogue will be available. When the Global CMT Project 'upgrades' to a new 3-D model, so will the near real-time system.

ACKNOWLEDGMENTS

REFERENCES

Amante, C. & Eakins, B., 2009. ETOPO1 1 Arc-minute global relief model: procedures, data sources and analysis, Tech. rep., NOAA.

Bassin, C., Laske, G. & Masters, G., 2000. The current limits of resolution for surface wave tomography in North America, in *EOS, Trans. Am. geophys. Un.,* **F897,** 81.

Chaljub, E., Capdeville, Y. & Vilotte, J.P., 2003. Solving elastodynamics in a fluid-solid heterogeneous sphere: a parallel spectral-element approximation on non-conforming grids, *J. Comp. Phys.,* **187**(2), 457–491.

Dahlen, F.A. & Tromp, J., 1998. *Theoretical Global Seismology,* Princeton Univ. Press, NJ, USA.

Deville, M.O., Fischer, P.F. & Mund, E.H., 2002. *High-Order Methods for Incompressible Fluid Flow,* Cambridge Univ. Press, Cambridge, UK.

Durek, J. & Ekström, G., 1996. A radial model of anelasticity consistent with long period surface wave attenuation, *Bull. seism. Soc. Am.,* **86,** 144–158.

Dziewoński, A. & Anderson, D., 1981. Preliminary reference Earth model, *Phys. Earth planet. Inter.,* **25,** 297–356.

Dziewoński, A. & Woodhouse, J.H., 1983. Studies of the seismic source using normal-mode theory, in *Earthquakes: Observation, Theory and Interpretation: Notes from the International School of Physics "Enrico Fermi" (1982: Varenna, Italy),* Vol. LXXXV, pp. 45–137, eds Kanamori, H. & Boschi, E., North-Holland Pub., Amsterdam, The Netherlands.

Dziewoński, A., Chou, T.-A. & Woodhouse, J.H., 1981. Determination of earthquake source parameters from waveform data for studies of global and regional seismicity, *J. geophys. Res.,* **86**(B4), 2825–2852.

Dziewoński, A.M. & Romanowicz, B., 2007. Seismology and the Structure of the Earth: Overview, in *Treatise on Geophysics,* pp. 1–30, ed. Schubert, G., Elsevier, The Netherlands.

Dziewoński, A.M., Hager, B.H. & O'Connell, R.J., 1977. Large-scale heterogeneities in the lower mantle, *J. geophys. Res.,* **82,** 239–255.

Gilbert, F., 1971. Excitation of normal modes of the Earth by earthquake sources, *Geophys. J. R. astr. Soc.,* **22,** 223–226.

Goldstein, P., Dodge, D., Firpo, M. & Minner, L., 2003. SAC2000: Signal processing and analysis tools for seismologists and engineers, in *International Handbook of Earthquake and Engineering Seismology, Part B,* eds Lee, W.H.K., Kanamori, H., Jennings, P.C. & Kisslinger, C., Vol. 81 of the International Geophysics Series, pp. 1613–1614, Academic Press, London, UK.

Grand, S.P., van der Hilst, R.D. & Widiyantoro, S., 1997. Global seismic tomography: a snapshot of convection in the Earth, *GSA Today,* **7,** 1–7.

Komatitsch, D. & Tromp, J., 1999. Introduction to the spectral element method for three-dimensional seismic wave propagation, *Geophys. J. Int.,* **139,** 806–822.

Komatitsch, D. & Tromp, J., 2002a. Spectral-element simulations of global seismic wave propagation—I. Validation, *Geophys. J. Int.,* **149,** 390–412.

Komatitsch, D. & Tromp, J., 2002b. Spectral-element simulations of global seismic wave propagation—II. Three-dimensional models, oceans, rotation and self-gravitation, *Geophys. J. Int.,* **150,** 308–318.

Komatitsch, D. & Vilotte, J.-P., 1998. The spectral element method: An efficient tool to simulate the seismic response of 2D and 3D geological structures, *Bull. seism. Soc. Am.,* **88,** 368–392.

Komatitsch, D., Labarta, J. & Michéa, D., 2008. A simulation of seismic wave propagation at high resolution in the inner core of the Earth on 2166 processors of MareNostrum, *Lecture Notes Comput. Sci.,* **5336,** 364–377.

Komatitsch, D., Michéa, D. & Erlebacher, G., 2009. Porting a high-order finite-element earthquake modeling application to NVIDIA graphics cards using CUDA, *J. Parall. Distrib. Comput.,* **69**(5), 451–460.

Komatitsch, D., Erlebacher, G., Göddeke, D. & Michéa, D., 2010. High-order finite-element seismic wave propagation modeling with MPI on a large GPU cluster, *J. Comput. Phys.,* **229,** 7692–7714, doi:10.1016/j.jcp.2010.06.024.

Kustowski, B., Ekström, G. & Dziewoński, A.M., 2008. Anisotropic shear-wave velocity structure of the Earth's mantle: a global model, *J. geophys. Res.,* **113,** B06306, doi:10.1029/2007JB005169.

Lee, S.-J., Chen, H.-W., Liu, Q., Komatitsch, D., Huang, B.-S. & Tromp, J., 2008. Three-dimensional simulations of seismic-wave propagation in the Taipei basin with realistic topography based upon the spectral-element method, *Bull. seism. Soc. Am.,* **98**(1), 253–264.

Montelli, R., Nolet, G., Dahlen, F.A., Masters, G., Engdahl, E.R. & Hung, S.-H., 2004. Finite-frequency tomography reveals a variety of plumes in the mantle, *Science,* **303,** 338–343.

Wessel, P. & Smith, W.H.F., 1991. Free software helps map and display data, *EOS, Trans. Am. geophys. Un.,* **72**(41), 441ff.

Woodhouse, J.H. & Dziewoński, A.M., 1984. Mapping the upper mantle: three-dimensional modeling of Earth structure by inversion of seismic waveforms, *J. geophys. Res.,* **89,** 5953–5986.